Phase stability of Fe-5at%Cr and Fe-10at%Cr films under Fe$^+$ ion irradiation

K Mergia[1,6], E O Tsompopoulou[1,2], S Dellis[1], C H Marrows[2],
I Michelakaki[1], C Kinane[3], A Caruana[3], S Langridge[3], A P Douvalis[4],
C Cabet[5] and S Messoloras[1]

[1] Institute for Nuclear and Radiological Science and Technology, Safety and Energy,
National Centre for Scientific Research 'Demokritos', 15310 Agia Paraskevi, Greece
[2] School of Physics and Astronomy, University of Leeds, Leeds LS2 9JT, United Kingdom
[3] Rutherford Appleton Laboratory, ISIS Neutron And Muon Source, Oxon, OX11 0QX, United Kingdom
[4] Physics Department, University of Ioannina, 45110 Ioannina, Greece
[5] DEN, Service de Recherches de Métallurgie Physique, CEA, Université Paris-Saclay, F-91191
Gif-sur-Yvette, France

E-mail: kmergia@ipta.demokritos.gr (KMergia)

CrossMark

Abstract

This work is within the objective of understanding the effects caused to Fe–Cr alloys by fast Fe ion irradiation. As the penetration length of Fe ion is of the order of hundreds of nanometers, 70 nm Fe-5at%C and Fe-10at%Cr films were irradiated at room temperature with 490 keV Fe$^+$ ions at increasing fluence corresponding to a maximum damage of 50 displacements per atom (dpa). In Fe-5at%Cr alloy the Cr solute concentration remains unaltered even after a damage of 50 dpa. In the 10at%Cr the Cr solute concentration is reduced, with the increase of damage, asymptotically to a value of 7.2 at%.

Keywords: ion irradiation, Fe–Cr alloys, magnetism, polarised neutron reflectivity, Cr precipitation

(Some figures may appear in colour only in the online journal)

Introduction

Understanding the radiation effects of energetic ions and neutrons on steel has considerable scientific interest and additionally important technological impact related to energy production by fusion [1–4]. These two aspects are interrelated, as a basic understanding of the phenomena will promote the development of radiation resistant materials necessary for the implementation of the international plans for a fusion reactor in the next twenty years.

For fusion energy applications, ferritic/martensitic Fe–Cr steels are candidate structural materials [2–4]. In a fusion reactor, these materials will be exposed to significant fluxes of highly energetic neutrons. Currently available alloys are unable to withstand these severe operational conditions expected in fusion power plants. Therefore, experimental investigations of irradiation effects on Fe–Cr binary alloys coupled with the theoretical modelling is of paramount importance for the development of radiation resistant complex steels.

Addition of Cr to pure Fe suppresses radiation-induced swelling by an order of magnitude [5]. Fe–Cr alloys of concentrations of 3–9 wt% Cr exhibit minimal neutron radiation-induced swelling rates. The minimum Ductile to Brittle Transition Temperature (DBTT) occurs at 9 wt% Cr, and the maximum corrosion resistance occurs at Cr content larger than 10 wt%. As a consequence, most steels considered as candidate structural materials in future fusion applications contain around 9 wt% Cr [2].

The experimental studies conducted so far on Fe–Cr-based steels refer mainly to the microstructural investigation of the neutron irradiation induced effects using a suite of experimental techniques including transmission electron microscopy (TEM) [6–8], atom probe tomography (APT) [9–13],

---

[6] Author to whom any correspondence should be addressed.

1

positron annihilation spectroscopy (PAS) [14, 15] and small angle neutron scattering (SANS) [16, 17].

Magnetic structure is an important aspect in understanding the radiation effects as important theoretical work has proved [18, 19]. In the literature, there are a limited number of investigations dealing with the magnetic effects caused by ion irradiation on Fe or Fe–Cr alloys [20–23]. Irradiation with 490 keV Fe^+ at 300 K induces drastic changes in the magnetic and structural properties (lattice constant and grain size) of polycrystalline Fe films [24, 25]. An enhancement of the Fe magnetic moment was observed which was attributed to the presence of sub-nanometer vacancy clusters. In addition, time relaxation phenomena of the magnetic moment were observed linked with the lifetime of the vacancy clusters [25]. Furthermore, in 200 nm thick Fe films, where both radiation damage and implantation effects take place, polarised neutron reflectivity (PNR) measurements revealed the presence of a magnetic depth profile depending on the type of defect created [24]. Significant magnetic hardening and a drastic change in domain structures were found in Fe–Cr single crystals at high temperature (478 K) irradiation and these findings were related to the formation of chromium-rich precipitates [20].

The main features of the 14 MeV neutron-induced radiation damage in the materials can be studied by employing self-ion irradiation [26, 27] as the lattice damage is produced by the neutrons knocking out atoms (primary knock-on atoms (PKA)) from their lattice positions and these PKA produce the damage. Therefore, self-ion irradiation replicates the starting interaction of the material damage produced by neutrons. The neutrons produce PKA of different energies, helium, hydrogen and transmutation products and all these produce multiple interaction paths and structures. This complexity renders difficult the attribution of the irradiation induced alteration of a macroscopic property (e.g. mechanical properties) to a specific contribution of an interaction path or generated microstructure (e.g. voids, dislocations, agglomerates). All these complexities can be avoided for self-ion irradiations as the energy of the self-ion imitating the neutron produced PKA is well defined and no transmutations occur. In addition, a wide choice of ion energies and dose rates are available for a methodical study of the damage. Therefore, the experimental results on the damage produced by energetic ions can provide deep insight on the radiation effects and there are a rewarding test bed for models and theoretical descriptions.

To a large degree the findings of self-ion irradiation may be extended to neutron ones provided that the differences between them are considered [28]. In neutron irradiation experiments He or other induced by transmutation impurities may play an important role for example in the evolution of the binary alloy system. The mean free path for neutrons is much larger than for ions so larger volumes with a wide range of deposited energies participate in the phenomena. Furthermore, the damage rates achieved with ions can be much larger than with neutrons. It has to be stressed that interstitials produced by implantation have to be avoided as they introduce an extra complexity. The requirement for employing specific energy of the impinging ion and for minimization of the implantation

effects necessitates the use of the material in thin film form. From the well defined energy of Fe ions the production of vacancy, defects and more complex aggregates can be evaluated by theoretical models. For modelling purposes thin films also provide a small volume with well defined boundaries and long range migrations do not need to be taken into account. For these reasons we have initiated a study of Fe ion irradiation effects initially of Fe films which is now extended to Fe–Cr alloy films.

Above we have demonstrated the advantageousness of the employment of ion irradiations instead of neutrons and of the thin film structures. Next the scientific questions addressed in this work will be detailed. It is questionable whether the phase diagram of Fe–Cr alloys remains the same under irradiation. Based on TEM observation of a' finely dispersed precipitates in the bulk and not attached to radiation defects such as dislocation loops or voids, it has been claimed that the ordering process can only be accelerated by irradiation (enhanced diffusion) and not induced by it [29]. This standpoint has been criticized as ignoring ballistic mixing which would dissolve the precipitates [30]. The thermodynamics and kinetics of the demixing process is a challenging problem, even without irradiation, as this system exhibits a unique inversion between ordering and segregation tendencies versus Cr content [31] and also magnetic [32, 33] and vibrational effects [34, 35] influence both the thermodynamic and diffusion properties of the system.

Decomposition occurring during thermal aging is typically occurring between 773 and 813 K, temperatures at which the thermal diffusion is adequate to drive it. Under irradiation, short-range ordering or decomposition can be observed at even lower temperatures, because the point defect supersaturation accelerates diffusion processes i.e. radiation induced segregation (RIS). RIS is the process by which the composition of an alloy is altered due to preferential participation of certain species with the vacancy and/or interstitial flux to sinks. Sinks pre-exist of any irradiation but mainly are created during the irradiation as vacancy/interstitial clusters or in the form of extended defects as dislocations and voids. The form of these aggregates observable by TEM depends on local equilibrium conditions and sinks structure and geometry. However, it is of paramount importance the determination of the global equilibrium conditions which are reflected by the solute Cr content in the matrix after irradiation. This is what exactly the present work determines as a function of the Fe^+ ion dose or displacements per atom. To this end two thin films are selected with Cr content at 5 and 10 at%. The former concentration is believed to lie outside the solvus whereas the later within the solvus area [36]. In principle, under heat treatment at a temperature in which the thermal diffusion is adequate, the Fe-5at%Cr alloy is expected to remain unchanged (no precipitation) whereas the solute concentration of the Fe-10at%Cr is expected to decrease as precipitates will be formed. Further, in order to observe only kinetics arising from irradiation induced or enhanced diffusion, the irradiation temperature of 300 K is used. At this temperature the thermal diffusion is extremely slow, thus no agglomeration without irradiation is expected.

Table 1. Irradiation time, fluence, dose and dose rate of the 490 keV Fe^+ ion irradiations.

Sample	Irrad. time (min)	Fluence (ions cm^{-2})	R_t dose (dpa)	Average dose rate (dpa min^{-1})
Fe-5at%Cr on MgO(1 0 0)	120	1.22×10^{16}	25	0.21
	245	2.45×10^{16}	50	
Fe-10at%Cr on MgO(1 0 0)	14.2	1.45×10^{15}	3	
	28.0	2.93×10^{16}	6	
Fe-10at%Cr on Si/SiO$_2$	27.4	2.93×10^{15}	6	
	114.3	1.22×10^{16}	25	
	228.0	2.45×10^{16}	50	

Materials and experimental methods

Sample fabrication and characterization

Fe–Cr alloy films with nominal Cr content of 0, 5, 10 and 15 at% Cr, having a thickness of around 70 nm, were fabricated on MgO(1 0 0) and Si/SiO$_2$ (300 nm) substrates using DC magnetron sputtering and high purity $Fe_{100-x}Cr_x$ ($x = 5, 10, 15$) (99.95%), Fe (99.99%) and Cr (99.95%) targets. The thickness of the films was controlled by calibrating the deposition rate using x-ray reflectivity measurements which provide with very high accuracy the film thickness. The concentrations of 0, 5 and 15 at% are used at their unirradiated state for calibration of the Cr content against magnetic per atom moment value (see the Results section below). The substrates were kept at room temperature during deposition. At this growth temperature, a textured polycrystalline FeCr film is expected to grow on MgO(1 0 0) due to the good lattice match of bcc Fe(Cr) with MgO(1 0 0) whereas no preferential orientation is expected for the growth of FeCr on top of the amorphous SiO$_2$ layer of Si/SiO$_2$ substrate. For the FeCr films deposited on MgO(1 0 0), the substrates were additionally annealed at 700 °C for 1 h under vacuum in order to enhance the textured growth. Liquid nitrogen circulation was used to reduce the water partial pressure in the sputtering chamber. On top of the FeCr films deposited at room temperature a nominally 4–5 nm thick Cr cover layer was deposited to prevent FeCr oxidation. This upper layer oxidizes and acts as a passivation layer that prevents the oxidization of the FeCr layer. The base pressure during deposition was 9×10^{-8} Torr, the power 8 Watt, the sputtering gas pressure 5.2×10^{-3} Torr and the deposition rate 0.37 Å s^{-1}.

The Cr content of the $Fe_{100-x}Cr_x$ films was verified by x-ray fluorescence (XRF) spectroscopy measurements and it was found to be 5.7 ± 0.2, 9.7 ± 0.2 and 13.7 ± 0.3 at% for $x = 5, 10$ and 15 respectively.

The crystalline and layered structure of the as fabricated films was investigated using x-ray diffraction (XRD) and x-ray reflectivity (XRR) measurements using Bruker D8 diffractometer with a Cu K$_a$ x-ray source and a parallel beam stemming from a Göbbel mirror. From the fitting of the XRR measurements using LEPTOS R software structural parameters as the film thickness, density and roughness were determined. The FeCr film thickness varied between 70 and 73 nm. The FeCr film density was almost the same (7.5 g cm^{-3}) for all the samples. Also the chromium oxide thickness was determined of around 3–4 nm. The roughness of the films was of the order of 0.5 nm and 2.5 nm for the films grown on MgO and Si/SiO$_2$ respectively.

The XRD measurements showed that the FeCr films crystallize in the bcc structure. Those deposited on Si/SiO$_2$(300 nm) substrates show no texture whereas those deposited on MgO(1 0 0) substrates present texture along the (1 0 0) direction of the substrate due to the lattice match of bcc FeCr with MgO(1 0 0).

The PNR experiments were carried out at POLREF facility, at the ISIS neutron and muon source, at Rutherford-Appleton Laboratory, UK. The measurements [37] were performed at room temperature in the presence of 1 T magnetic field applied in plane with the sample and perpendicular to the beam direction.

Irradiations

Irradiations with 490 keV Fe^+ ion beam were performed at the 3 MV Épiméthée accelerator, at the JANNuS facility [38] at CEA-Saclay using an ion flux of around 1.8×10^{12} ions (cm^2 s)$^{-1}$. The samples during the irradiation were placed under UHP vacuum (10^{-6} mbar) on a liquid nitrogen cooled flange to compensate for the heating induced by the beam and thus keeping the sample temperature at 25 °C. The ion beam was incident at 15° with the sample normal. The samples were irradiated for different times up to a fluence of 2.45×10^{16} ions cm^{-2}. The irradiation parameters are presented in table 1.

Results

Irradiations

The energy of 490 keV was chosen as the energy of the Fe^+ ions to bombard the samples. This energy corresponds to the mean energy of Primary Knock-on Fe Atoms produced from 14 MeV fusion neutrons. The penetration of 490 keV Fe^+ is around 400 nm. For depths larger than 100 nm implantation effects start to become significant, whereas for film thickness up to about 80 nm radiation damage effects are predominant.

In order to define the film thickness and the damage produced by 490 keV Fe^+ ions, simulations using the SRIM-2008 software [39] have been performed on Fe-5at%Cr and Fe-10at%Cr targets. For the displacement energy the value of 40 eV (ASTM standard, [40]) has been used. There are two
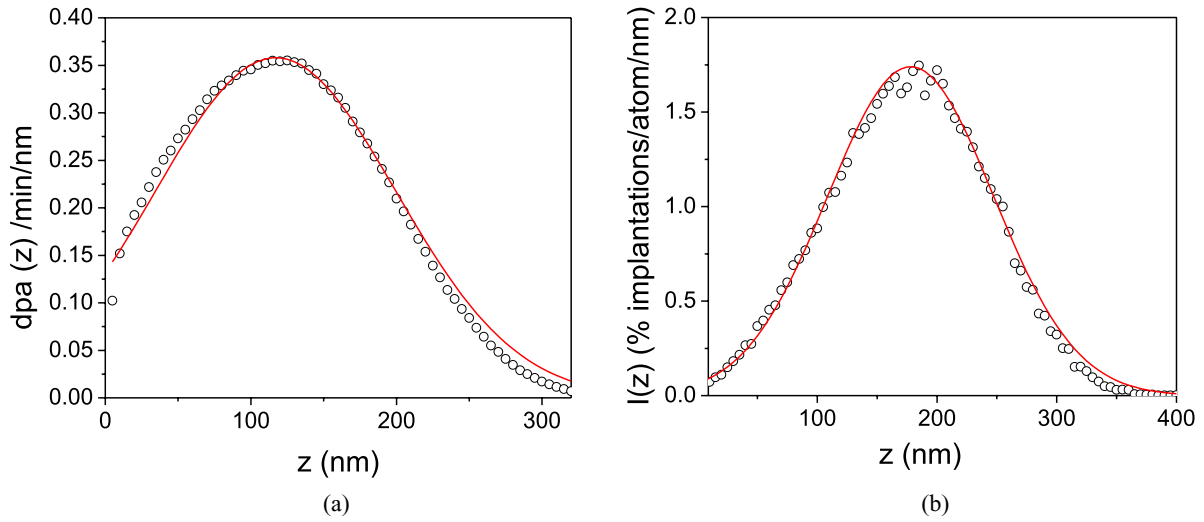
Figure 1. (a) Damage rate as a function of depth of Fe-10at%Cr films irradiated by 490 keV Fe + ions, computed by SRIM for a flux of 1.8×10^{12} ions (cm² s)⁻¹. Solid line: see text for details. (b) Percentage of implanted Fe ions over the number of atoms in the sample as a function of depth of Fe-10at%Cr films irradiated by 490 keV Fe + ions, computed by SRIM for 50 dpa and a flux of 1.8×10^{12} ions (cm² s)⁻¹. Solid line: see text for details.

main parameters which characterize the interaction of ion with matter: the damage produced and the number of ions implanted. Both parameters vary versus film depth.

The damage is characterized in terms of the average number of times that an individual atom is displaced from its lattice site i.e. 'displacements per atom' (dpa) and this unit is employed throughout this paper. In figure 1(a) the damage rate, r, in dpa per minute per nanometer for a flux of 1.8×10^{12} ions (cm² s)⁻¹ (that employed in our experiments) and for a Fe-10at%Cr film is depicted (the results for Fe-5at%Cr are very similar). In the same figure is shown a fitted Gaussian of the form

$$r = r_{max} \exp\left(-\left(\frac{z - z_0}{\sigma}\right)^2\right) \qquad (1)$$

where $r_{max} = 0.358$ dpa (nm min)⁻¹ the maximum damage rate, $z_0 = \sigma = 117$ nm the centre of the Gaussian having a Full Width Half Maximum (FWHM) equal to FWHM $= 2\sigma\sqrt{\ln 2}$. It is more convenient to characterize the damage rate produced in a film of thickness D by the mean damage rate, $\langle r \rangle$, defined as

$$\langle r \rangle = \frac{1}{D} \int_0^D r(z) \, \mathrm{d}z \qquad (2)$$

which for 70 nm film thickness is 0.21 dpa min⁻¹. The dose, R (table 1), is calculated by the equation $R = t_{irr} \langle r \rangle$ where t_{irr} is the time of irradiation.

The other parameter of interest is the percentage of implanted impinging Fe ions compared over the number of atoms in the sample. This is shown in figure 1(b) for irradiation of 4 h, i.e. time at which a sample of 70 nm will incur mean damage of around 50 dpa. Again the implanted ions can be fitted with a Gaussian with maximum height $I_{max} = 1.74\%$, centre at $z_0 = 178$ nm and width $\sigma = 98$ nm.

Summarizing the simulations depicted in figure 1 we may conclude that atomic displacements are the predominant mechanism up to the depth of about 100 nm while implantation
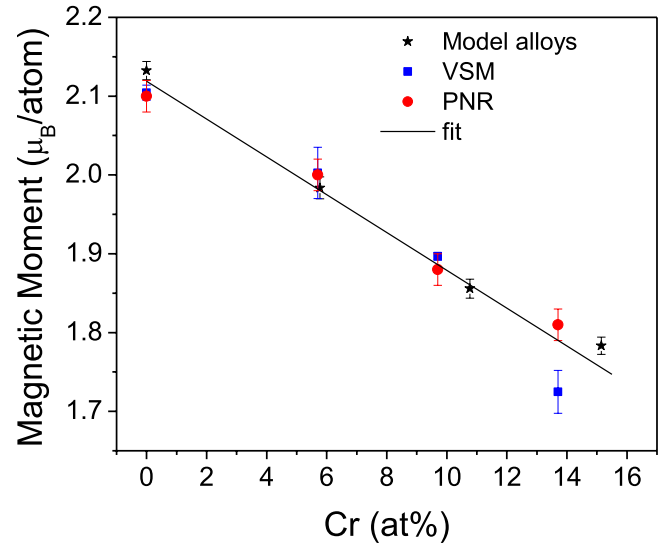

Figure 2. The magnetic moment per atom of the as-fabricated samples as a function of Cr content determined by both PNR and VSM measurements and the magnetic moment of FeCr bulk alloys [43] as determined by VSM. The solid line is a least squares fit to all the data.

effects become important for higher depths. Thus, FeCr films with thickness around 70 nm are used for the investigation of Fe⁺ ion irradiation damage effects on FeCr. The 490 keV Fe⁺ ions deposit 73% of their energy to Fe and Cr recoils while the remaining energy is dissipated to ionization and phonons.

The XRR and PNR measurements before and after irradiation did not show any significant changes of the FeCr film thickness and density. Also the thickness of the top protective chromium oxide layer is not altered by the irradiation. XRR show only a slight increase of the surface roughness of the chromium oxide which is further verified by AFM observations. Thus, it is concluded that sputtering effects arising from irradiation do not change the film structure.
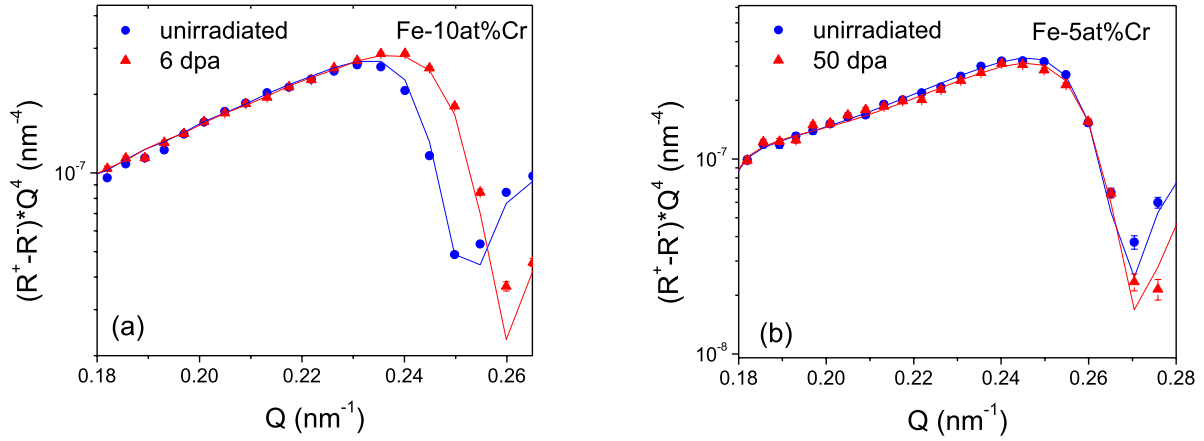
Figure 3. Spin asymmetry $(R^+ - R^-) Q^4$ at the critical edge. The solid lines are least squares fits to the data. (a) Fe-10at%Cr alloy unirradiated and irradiated at 6 dpa. (b) Fe-5at%Cr alloy unirradiated and irradiated at 50 dpa.

Dilute Cr determination by polarized neutron reflectivity (PNR)

The purpose of using polarized neutron reflectivity (PNR) measurements has been the determination of solute Cr concentration in the matrix after different irradiations and to investigate any depth dependence variation of this property. This is accomplished by determining the magnetization versus depth and using the methodology described below.

Initially a short description of the PNR technique [41] is given. A magnetic field parallel to the surface of the sample is applied in order to create a saturated long range order in the FeCr film. Neutrons are incident with their spin or their magnetic moment either parallel $(+)$ or antiparallel $(-)$ to the applied field. The neutron reflectivity is measured for the two states of the neutron spin and it is denoted as R^+, R^-. The interaction potential is $V_{\text{nuclear}} \pm \mu \langle M_z(z) \rangle$ where V_{nuclear} the nuclear part, μ the neutron magnetic moment, $\langle M_z(z) \rangle$ the sample magnetization versus depth, z, (see equation (3)) and the $\pm$ sign refers to the spin state of the neutron. The measured reflectivity corresponds to a mean magnetization defined as

$$\langle M_z(z) \rangle = \frac{\int_{z-\delta z/2}^{z+\delta z/2} \mathrm{d}z' \int \int_S M(\mathbf{r}) \cos \theta(\mathbf{r}) \, \mathrm{d}S}{\delta z \, S}. \quad (3)$$

$M(\mathbf{r})$ is the local magnetic moment, S the sample surface, $\theta(\mathbf{r})$ the angle of the local magnetic moment with the axis of quantization (magnetic field) and δz the resolution which is of the order of 1 nm. For a random orientation of local magnetization moments, $M(\mathbf{r})$, equation (3) gives zero, thus R^+, R^- are equal. In the ferromagnetic state of random bcc Fe–Cr alloys, the Cr magnetic moment is aligned antiparallel to the Fe magnetic moment, as well as to the global magnetization vector [42]. Therefore for this case we will have

$$\langle M_z(z) \rangle \propto -x_{\text{Cr}} \mu_{\text{Cr}} + (1 - x_{\text{Cr}}) \mu_{\text{Fe}} \quad (4)$$

where x_{Cr} the atomic fraction of Cr and $\mu_{\text{Cr}}, \mu_{\text{Fe}}$ the atomic magnetic moments of Cr and Fe atoms, respectively. In case that within the matrix exist paramagnetic clusters or ferromagnetic clusters randomly oriented within the macroscopic volume $\delta z S$ (equation (3)) these will not contribute to the averaged magnetization. Short range order does not contribute to

the observed reflectivity, whereas long range variations in the z direction are observable. Therefore paramagnetic Cr rich clusters or short range magnetization variation due to Cr pairing are not observed. In conclusion the PNR reflects solely the magnetic moment of the FeCr matrix averaged in the long range.

The analysis of the PNR spectra consist in deducing both the nuclear density (i.e. atomic species and the relative concentrations) and the magnetization of the sample versus depth. For this purpose GenX software [43] was used. It must be emphasized that both the nuclear density and the magnetic moment are determined in absolute values and thus we evaluate the magnetic moment per atom which in correspondence with equation (4) can be written as

$$m(\mu_{\text{B}}/at) = m_0 - k \cdot x_{\text{Cr}}(at\%) \text{ or } x_{\text{Cr}}(at\%) = A \left(\frac{at\%}{\mu_{\text{B}}/at} \right)(m_0 - m) \quad (5)$$

where x_{Cr} is the Cr concentration in at%. In order to determine the Cr solute concentration in the film we need to validate the reasoning outlined above and also to experimentally determine the constants m_0 and k. For this we have used three sets of measurements: (a) bulk model FeCr alloys of different concentrations and VSM measurements [44], (b) thin film FeCr alloys and VSM measurements and (c) the same thin films as in (b) and PNR measurements. The results of the three sets of measurements are shown in figure 2. It is noticed that there is a good agreement among the different sets of measurements and the constants determined by least squares fit to all the data are $m_0 = 2.12 \pm 0.01 \ \mu_{\text{B}}/at$ and $A = 41.0 \pm 1.4 \ (at\%/\mu_{\text{B}}/at)$. It is noticed that the value of m_0 corresponds to the magnetic moment of Fe at room temperature. The error in determining the Cr concentration in the matrix is $\delta x_{\text{Cr}}/x_{\text{Cr}} = 3.4\%$.

In order to show the sensitivity of the PNR technique in determining the solute Cr concentration, in figure 3(a) we present the measured difference of $R^+ - R^-$ for the unirradiated sample and that irradiated to a damage of 6 dpa for the 10 at% Cr system around the critical edge, whereas in figure 3(b) this difference for the 5 at%Cr system is depicted for the unirradiated sample and that irradiated at 50 dpa. The reflectivities have been multiplied by Q^4 ($Q = \frac{4\pi \sin \theta}{\lambda}$, 2θ the scattering angle and λ the neutron wavelength) in order, by removing
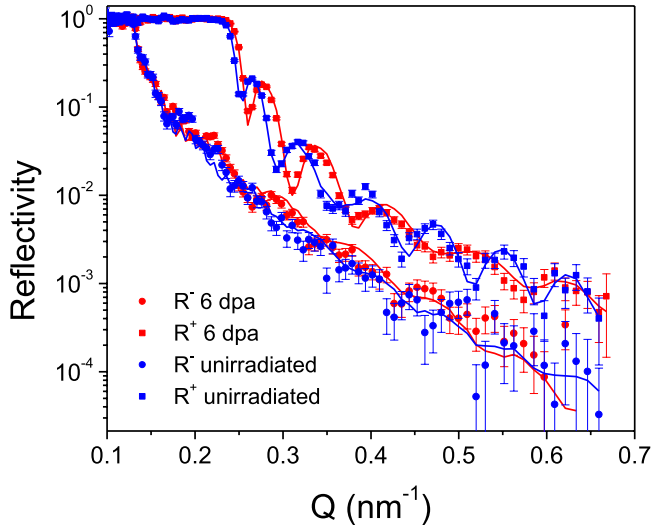
Figure 4. PNR spectra for the unirradiated and the 6 dpa irradiated Fe-10at%Cr alloy. The solid lines are least squares fits to the data.

Figure 5. The magnetic moment versus dose for Fe-10at%Cr determined by least squares fit to the reflectivity data (see for example figure 4).

the asymptotic behaviour of the reflectivity, to demonstrate the effect of the irradiation on the magnetic structure of the Fe-10at%Cr film. The difference of the spin up minus spin down reflectivity is very sensitive to the sample magnetization and it is zero for zero magnetization. The data around the critical edge, presented in figure 3, depend only on the value of the mean magnetization $\langle M \rangle$

$$\langle M \rangle = \frac{1}{D} \int_0^D \langle M_z(z) \rangle \, dz \qquad (6)$$

where D is the film thickness. The reflectivity at higher Q values depends on the mean magnetization, its dependence versus depth and on the film structure. The usual procedure for deriving magnetic and structural parameters from PNR measurements is to devise a magnetization and structure versus depth profile and by least squares fitting to obtain the magnetic and the structural parameters of the model.

In figure 4 the R^+ and R^- reflectivities for the Fe-10at%Cr film irradiated up to 6 dpa are shown. Together with the data points the least squared fitted curves are presented. In the fitting procedure [41] both the magnetization versus depth and film density versus depth may be incorporated. The film density derived by the fitting is very similar to that determined by XRR and very close to the nominal one. In all the samples the reflectivity data show that there is no measurable depth dependence of the magnetization (for example in [24] magnetization difference of 0.78 μ_B/atom was measured by PNR). Therefore, the only parameter describing the magnetic state is that of the mean magnetization and as film thickness and density have been obtained by the fitting we can calculate the magnetic moment per atom (absolute determination).

The derived magnetic moments versus dose (dpa) are presented in figure 5. It is observed that the magnetic moment increases up to 6 dpa and for higher doses it remains almost constant and equal to 1.95 μ_B/atom. The variation of the magnetic moment versus dose does not seem to depend on the microstructure (polycrystalline or highly textured) of the

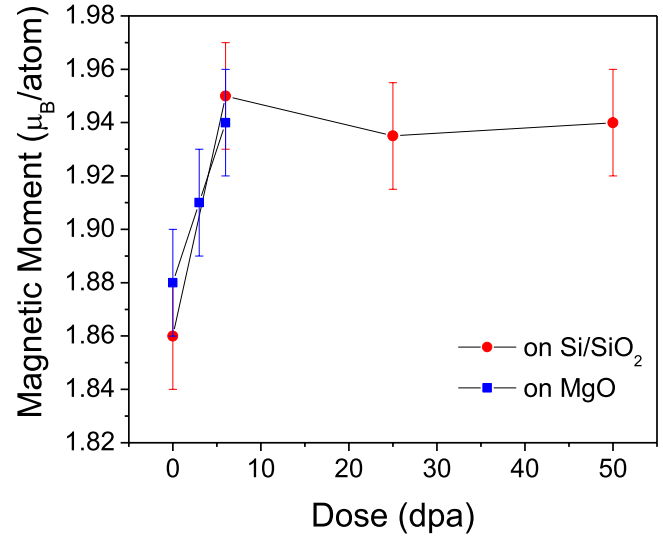Fe-10at%Cr alloy film since there is no observable difference between films grown on either MgO or silicon substrates.

This increase of the magnetic moment per atom observed for the Fe-10at%Cr alloy is not observed in the case of the Fe-5at%Cr alloy system. Indeed, no change of the magnetic moment is observed at the irradiation doses of 25 and 50 dpa. This is demonstrated in figure 3(b) where the measurements of the unirradiated sample and that irradiated to 50 dpa coincide at the critical edge.

Using equation (5), the least squares determined constants and the magnetic moments determined by PNR (figure 5) the Cr content in the FeCr matrix was determined. The Cr content of the Fe-10at%Cr and for the different doses is depicted in figure 6. The experimental Cr concentration in the matrix versus dose in dpa, $C(d)$, has been fitted using the equation (solid line in figure 6)

$$C(d) = C_0 - C_\infty \left(1 - e^{-\frac{d}{d_0}} \right) \qquad (7)$$

where C_0 is the initial concentration, $C_{eq} = C_0 - C_\infty$ the equilibrium concentration and d_0 the radiation damage saturation constant. The values found by least squares fitting are $C_0 = 10.6 \pm 0.4$ at%, $C_\infty = 3.4 \pm 0.3$ at% and $d_0 = 2.2 \pm 0.7$ dpa. The corresponding equilibrium concentration of solute Cr in the matrix is $C_{eq} = 7.2 \pm 0.5$ at%

Discussion and conclusions

Films of Fe-5at%Cr and Fe-10at%Cr of thickness around 70 nm have been irradiated by 490 keV Fe^+ ions to different damage levels from 3 to 50 dpa. The energy of 490 keV Fe^+ ions corresponds to the mean energy of the primary Fe knock-ons produced by 14 MeV fusion neutrons. The films before and after irradiations have been characterized by XRF spectroscopy (chemical composition), XRR (film structure and density) and XRD (crystal structure). The Cr total content in
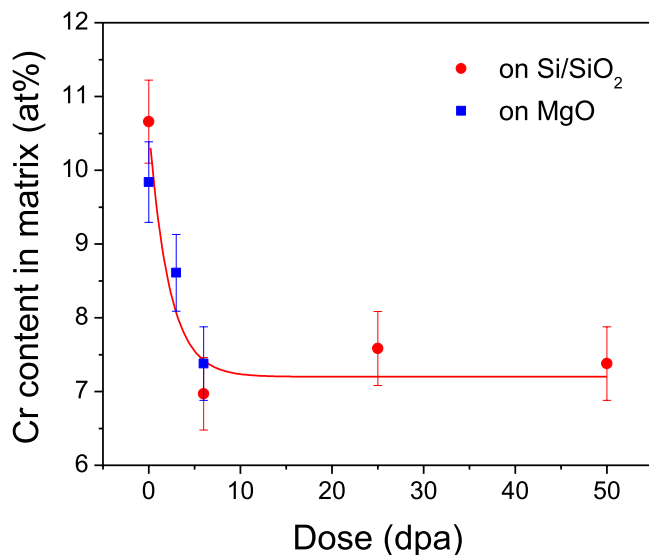
Figure 6. The Cr content in the FeCr matrix versus dose, for the Fe-10at%Cr alloy, as calculated from the magnetic moments of figure 5 and equation (5). The continuous line is a least squares fit to the data (equation(7)).

the film as determined by XRF spectroscopy after irradiation remains the same as the initial one. XRD data show that the crystal structure remains unaltered even after 50 dpa irradiation. Structural stability is also observed by XRR measurements from which it is concluded that both the density and the film thickness are not influenced by the irradiation. Also the two interfaces i.e. the one between the film and the top chromium oxide protection layer and the other between the film and the substrate (SiO_2 or MgO) remain sharp i.e. there is no inter-diffusion or intermixing. From the above experimental facts an important conclusion can be reached that the effects to be discussed below occur within the FeCr film.

PNR has been implemented to determine the magnetic moment of the films before and after the irradiation. Within the context of this work the advantages of PNR is the absolute determination of the magnetic moment versus film depth. The measured magnetic moment of the FeCr films, as shown above, can be transformed to Cr solute concentration versus depth with an accuracy of around 3%. With this procedure we are able to study the phase transformation induced by ion irradiation i.e. changes of the Cr solute concentrations versus depth with a resolution of the order of 1 nm. PNR is a non-destructive technique and no special treatment of the samples before or after irradiation is required thus changes of the state of the sample inherent in other techniques are avoided.

In the Fe-5at%Cr alloy even after a damage of 50 dpa no change of the diluted Cr concentration has been observed which remains 5 at%. In the Fe-10at%Cr alloy after a damage of 3 dpa the solute Cr content in the matrix is reduced to around 8.7 at%. Further irradiation to 6 dpa reduces the Cr content to 7.4 at%. Further damage, up to 50 dpa, does not change the Cr content in the matrix (see figure 6). The Cr depletion versus dose in the Fe-10at%Cr alloy is described by equation (7).

The Fe rich solvus at 300 K is around 5 ± 2 at% Cr [30]. Therefore we expect the Fe-5at%Cr alloy to be

thermodynamically stable whereas the Fe-10at%Cr to be unstable i.e. to decompose to *a* and *a′* phases. However, decomposition of this alloy into two phases does not occur at room temperature as the diffusion is very slow and in order to realize this effect heat treatments at higher temperatures are required. The higher temperature ageing results in the formation of *a′* precipitates with body centered cubic lattice ([45–48] and references therein). Primary *a′* nuclei are finely dispersed particles of nanometric size typically having about 85%–95% of Cr in them [17]. These nanometre-sized Cr-rich precipitates are the cause of the hardening and embrittlement observed in ferritic martensitic (FM) steels after thermal ageing (so-called '475 °C embrittlement' [49, 50]) and at 250 °C under irradiation [51]. Precipitation hardening is therefore a problem that affects FM steels over a wide range of Cr concentrations and temperatures and it is of practical interest for technological applications [52, 53].

In summary of the above paragraph the Fe-5at%Cr alloy is at thermodynamic equilibrium whereas the Fe-10at% is not. Under irradiation the excess vacancies and interstitial produced lead to an enhanced Cr diffusion so the system moves to its equilibrium state. In this picture it should not be ignored that under irradiation the thermodynamic system is not that of two phases (Fe rich or Cr rich phases) but the system is more complicated as vacancies and interstitials and their clusters have to be taken into account. Radiation-accelerated formation of Cr-rich bcc precipitates is indeed known to occur within a certain range of temperature and Cr concentration over 9 at%, depending on dose and dose rate, in neutron irradiated Fe–Cr alloys [6–17, 51, 54]. According to the literature the formation of *a′* precipitation in self-ion irradiation of Fe–Cr alloys is an open question. In our study the observed Cr depletion from the matrix could be also attributed to either Cr clustering with contaminant carbon or nitrogen solutes or Cr clustering either at dislocation loops or grain boundaries. Both phenomena have been observed in ion irradiated Fe–Cr alloys [28, 55].

From the above discussion a general picture explaining the experimental results emerges. Ion irradiation produces excess vacancies and interstitials which in their turn produce enhanced Cr diffusion. The observed Cr removal from the matrix implies that Cr segregates forming small or large clusters. In a bulk alloy segregation regions which minimize the free energy for second phase formation are solute atoms, dislocations and grain boundaries. The irradiation introduces additional nucleation centres as amorphous areas, voids and clusters of vacancies and interstitials. Once the solute concentration in the matrix is close to equilibrium the further decomposition occurs via an Ostwald type ripening mechanism [56, 57]. In this low supersaturation regime the further decrease of Cr solute concentration to equilibrium is slow and the smaller agglomerates dissolve in favour of the larger ones, which grow further. The Cr solute content versus damage in figure 6 for the Fe-10at%Cr alloy is consistent with the above desription. In the Fe-5at%Cr alloy no Cr solute reduction is observed. The diffusion also in this case is enhanced but any small agglomerates that may be formed by chance or by 'ballistic' effects are

energetically unfavourable and are dissolved. Ballistic has the meaning that irradiation 'mixes up' the atoms, each atom has been moved on average 0.2 times per min, and without doubt Cr atoms come close to form by chance crowdions or clusters.

It is worth examining the near to equilibrium state of the Fe-10at%Cr which is attained after 6 dpa damage or irradiation time of 30 min. The near equilibrium term means that the system asymptotically, as it is described by equation (6), tends to the equilibrium solute Cr concentration which has been determined to be around 7.2 at%. This corresponds with that given from the phase diagram at room temperature (see phase diagram of Bonny *et al*. [36]). This equilibrium is not a simple thermodynamic equilibrium but it is more complex. Agglomerates of any size are dissolved by the Fe^+ ion bombardment, every minute 20% of the atoms are displaced. The mean time needed to displace all the 3 at% Cr in agglomerates is the less than 5 min.

The stability of the system described above at first glance seems peculiar. However, looking close to the radiation damage of the 490 keV Fe^+ ions, the understanding of this dynamic equilibrium is feasible. Without doubt there is a large number of Cr displacements from the agglomerates. However, the mean kinetic energy of these atoms is around 1.70 keV. The mean range of these atoms is around 1.2 nm, i.e. around four jumps. As also the number of vacancies is high around the Cr agglomerate, then the probability of the displaced atoms returning to the agglomerate is high. Within this discussion the picture of the so called agglomerate emerges. Within the agglomerate region the concentration of Cr, vacancies and interstitials and any pairs of them remains constant. This dynamic stability is a function of the damage rate, energy of incident ions and solute concentration outside the agglomerate region.

Summary

Fe-10at%Cr and Fe-5at%Cr alloy films were irradiated at room temperature with 490 keV Fe + ions to a damage ranging from 3 to 50 dpa. Employing Polarised Neutron Reflectivity measurements the Cr solute in the matrix was determined. In Fe-5at%Cr alloy the Cr solute concentration remains unaltered even after a damage of 50 dpa. In the 10at%Cr the Cr solute concentration is reduced, with the increase of damage, asymptotically to a value of 7.2 at%. This value has been almost attained after a damage of 6 dpa. The reduction of Cr concentration in the matrix implies that the diluted in the matrix Cr atoms under the irradiation induced enhanced diffusion are transported and segregate into sinks within the matrix. The equilibrium Cr solute concentration, 7.2 at%, of the Fe-10at%Cr alloy under irradiation and that of the diluted Cr in the Fe-5at%Cr, remains unaltered by the irradiation and this is consistent with the phase diagram of Fe–Cr [30]. However, these two equilibria are not simple thermodynamic ones of *a* and *a'* phase. Under irradiation in each region of the alloy there is equilibrium of the concentrations of Cr, vacancies, interstitials and their pairs. In addition each region (either Cr or Fe rich) is in equilibrium with the adjacent regions. Of course this picture refers to space and time or ensemble average.

It is essential to stress the significance of self-ion irradiations on thin films for developing and testing theoretical models. The energy and fluence of the damage producing agent are well defined as its interactions with the material. Furthermore the interaction volume is small and defined by the film boundaries.

Acknowledgments

ORCID iDs

K Mergia https://orcid.org/0000-0002-2633-8750
S Dellis https://orcid.org/0000-0003-3299-1833
C H Marrows https://orcid.org/0000-0003-4812-6393
A Caruana https://orcid.org/0000-0003-0715-5876

References

[1] Knaster J, Moeslang A and Muroga T 2016 Materials research for fusion *Nat. Phys.* **12** 424–34
[2] Zinkle S 2005 Advanced materials for fusion technology *Fusion Eng. Des.* **74** 31–40
[3] Lässer R, Baluc N, Boutard J-L, Diegele E, Dudarev S, Gasparotto M, Möslang A, Pippan R, Riccardi B and van der Schaaf B 2007 Structural materials for DEMO: The EU development, strategy, testing and modelling *Fusion Eng. Des.* **82** 511–20
[4] Stork D *et al* 2014 Materials R&D for a timely DEMO: Key findings and recommendations of the EU Roadmap Materials Assessment Group *Fusion Eng. Des.* **89** 1586–94
[5] Little E A and Stow D A 1979 Void-swelling in irons and ferritic steels: II. An experimental survey of materials irradiated in a fast reactor *J. Nucl. Mater.* **87** 25–39
[6] Chen W Y, Miao Y, Gan J, Okuniewski M A, Maloy S A and Stubbins J F 2016 Neutron irradiation effects in Fe and Fe–Cr at 300 °C *Acta Mater.* **111** 407–16
[7] Bachhav M, Robert Odette G and Marquis E A 2044 α' precipitation in neutron-irradiated Fe–Cr alloys *Scr. Mater.* **74** 48–51
[8] Porollo S I, Dvoriashin A M, Vorobyev A N and Konobeev Yu V 1998 The microstructure and tensile properties of Fe–Cr alloys after neutron irradiation at 400 °C to 5.5–7. 1 dpa *J. Nucl. Mater.* **256** 247–53
[9] Kuksenko V, Pareige C and Pareige P 2012 Intra granular precipitation and grain boundary segregation under neutron irradiation in a low purity Fe–Cr based alloy *J. Nucl. Mater.* **425** 125–29

[10] Kuksenko V, Pareige C and Pareige P 2013 Cr precipitation in neutron irradiated industrial purity Fe–Cr model alloys *J. Nucl. Mater.* **432** 160–65

[11] Chen W Y, Miao Y, Wu Y, Tomchik C A, Mo K, Gan J, Okuniewski M A, Maloy S A and Stubbins J F 2015 Atom probe study of irradiation-enhanced α precipitation in neutron-irradiated Fe–Cr model alloys *J. Nucl. Mater.* **462** 242–49

[12] Bergner F, Pareige C, Kuksenko V, Malerba L, Pareige P, Ulbricht A and Wagner A 2013 Critical assessment of Cr-rich precipitates in neutron-irradiated Fe-12 At%Cr: comparison of SANS and APT *J. Nucl. Mater.* **442** 463–69

[13] Reese E R, Bachhav M, Wells P, Yamamoto T, Robert Odette G and Marquis E A 2018 On α' precipitate composition in thermally annealed and neutron irradiated Fe-9-18Cr alloys *J. Nucl. Mater.* **500** 192–8

[14] Lambrecht M and Malerba L 2011 Positron annihilation spectroscopy on binary Fe–Cr alloys and ferritic/martensitic steels after neutron irradiation *Acta Mater.* **59** 6547–55

[15] Kwon J, Toyama T, Kim Y-M, Kim W and Hong J-H 2009 Effects of radiation-induced defects on microstructural evolution of Fe–Cr model alloys *J. Nucl. Mater.* **386–8** 165–68

[16] Ulbricht A, Heintze C, Bergner F and Eckerlebe H 2010 SANS investigation of a neutron-irradiated Fe–9 at%Cr alloy *J. Nucl. Mater.* **407** 29–33

[17] Mathon M H, de Carlan Y, Geoffroy G, Averty X, Alamo A and de Novion C H 2003 A SANS investigation of the irradiation-enhanced A–α' phases separation in 7–12 Cr martensitic steels *J. Nucl. Mater.* **312** 236–48

[18] Derlet P M and Dudarev S L 2007 *Prog. Mater. Sci.* **52** 299–318

[19] Nguyen-Manh D, Pui-Wai M, Lavrentiev M Y and Dudarev S L 2015 *Ann. Nucl. Energy* **77** 246–51

[20] Kamada Y, Watanabe H, Mitani S, Mohapatra J N, Kikuchi H, Kobayashi S, Mizuguchi M and Takanashi K 2013 Ion-irradiation enhancement of materials degradation in Fe–Cr single crystals detected by magnetic technique *J. Nucl. Mater.* **442** S861–64

[21] Kamada Y, Watanabe H, Mitani S, Echigoya J, Mohapatra J N, Kikuchi H, Kobayashi S and Takanashi K 2011 Magnetic properties of ion irradiated epitaxial Fe films *J. Phys.: Conf. Ser.* **266** 012035

[22] Kamada Y, Watanabe H, Mitani S, Echigoya J-I, Kikuchi H, Kobayashi S, Yoshida N and Takanashi K 2009 Effects of room temperature heavy-ion irradiation on magnetic and electrical properties of a single crystalline iron thin film *Mater. Trans.* **50** 2134–8

[23] Park D G, Moon E J, Kim D J, Chi S H and Hong J H 2003 The change of saturation magnetization in neutron-irradiated low-alloy steel *Physica* B **327** 315–8

[24] Papamihail K, Mergia K, Ott F, Yves S, Speliotis T, Apostolopoulos G and Messoloras S 2016 Fe + ion irradiation induced changes in structural and magnetic properties of iron films *J. Nucl. Mater. Energy* **9** 459–64

[25] Papamihail K, Mergia K, Ott F, Serruys Y, Speliotis Th, Apostolopoulos G and Messoloras S 2016 Magnetic effects of self ion irradiation of Fe films *Phys. Rev.* B **93** 100404

[26] Nelson S, Mazey D J and Hudson J A 1970 The use of ion accelerators to simulate fast neutron-induced voidage in metals *J. Nucl. Mater.* **37** 1–12

[27] Was G S, Jiao Z, Getto E, Sun K, Monterrosa A M, Maloy S A, Anderoglu O, Sencer B H and Hackett M 2014 Emulation of reactor irradiation damage using ion beams *Scr. Mater.* **88** 33–36

[28] Hardie C D, Williams C A, Xu S and Roberts S G 2016 Effects of irradiation temperature and dose rate on the mechanical properties of self-ion implanted Fe and Fe–Cr alloys *J. Nucl. Mater.* **439** 33–40

[29] Bonny G, Terentyev D and Malerba L 2008 On the α-α' miscibility gap of Fe–Cr alloys *Scr. Mater.* **59** 1193–6

[30] Xiong W, Selleby M, Chen Q, Odqvist J and Du Y 2010 Evaluation of phase equilibria and thermochemical properties in the Fe–Cr system *Crit. Rev. Solid State Mater. Sci.* **35** 125–52

[31] Mirebeau I, Hennion M and Parette G 1984 First measurement of short-range-order inversion as a function of temperature in a transition alloy *Phys. Rev. Lett.* **53** 687–90

[32] Klaver T P C, Drautz R and Finnis M W 2006 *Phys. Rev.* B **74** 094435

[33] Olsson P, Abrikosov I A and Wallenius J 2006 Electronic origin of the anomalous stability of Fe-rich bcc Fe–Cr alloys *Phys. Rev.* B **73** 104416–8

[34] Fultz B, Anthony L, Robertson J L, Nicklow R M, Spooner S and Mostoller M 1995 *Phys. Rev.* B **52** 3280

[35] Swan-Wood T L, Delaire O and Fultz B 2005 *Phys. Rev.* B **72** 024305

[36] Bonny G, Terentyev D and Malerba L 2010 New contribution to the thermodynamics of Fe–Cr alloys as base for ferritic steels *J. Phase Equilibria Diffus.* **31** 439–44

[37] Mergia K, Messoloras S, Kinane C and Langridge D 2017 *Polarized neutron reflectivity investigation of Fe$^+$ ion irradiated FeCr films* (https://doi.org/10.5286/ISIS.E.86778276)

[38] Gentils A and Cabet C 2019 Investigating radiation damage in nuclear energy materials using JANNuS multiple ion beams *Nucl. Instrum. Methods Phys. Res.* B **447** 107–12

[39] Ziegler J F, Biersack J P and Littmark U 1985 *The Stopping and Range of Ions in Solids* (New York: Pergamon)

[40] ASTM International, ASTM Standard E693-94 1994 *Standard Practice for Characterising Neutron Exposure in Iron and Low Alloy Steels in Terms of Displacements per Atom (dpa)*

[41] Ankner J F and Felcher G P 1999 Polarized-neutron reflectometry *J. Magn. Magn. Mater.* **200** 741–54

[42] Korzhavyi P A, Ruban A V, Odqvist J, Nilsson J-O and Johansson B 2009 Electronic structure and effective chemical and magnetic exchange interactions in bcc Fe–Cr alloys *Phys. Rev.* B **79** 054202

[43] Björck M and Andersson G 2007 GenX: an extensible x-ray reflectivity refinement program utilizing differential evolution *J. Appl. Cryst.* **40** 1174–8

[44] Lavrentiev M Y, Mergia K, Gjoka M, Nguyen-Manh D, Apostolopoulos G and Dudarev S L 2012 Magnetic cluster expansion simulation and experimental study of high temperature magnetic properties of Fe–Cr alloys *J. Phys.: Condens. Matter* **24** 326001

[45] Fisher R M, Dulis E J and Carroll K G 1953 Identification of the precipitate accompanying 885F embrittlement in chromium steels *Trans. Am. Inst. Min. Metall. Pet. Eng.* **197** 690–5

[46] Miller M K 1989 Field evaporation and field ion microscopy study of the morphology of phases produced as a result of low temperature phase transformations in the iron chromium *Syst. Colloq. Phys.* **50** 247–52

[47] Bley F 1992 Neutron small-angle scattering study of unmixing in Fe–Cr alloys *Acta Metall. Mater.* **40** 1505–17

[48] Danoix F and Auger P 2000 Atom probe studies of the Fe–Cr system and stainless steels aged at intermediate temperature: a review *Mater. Charact.* **44** 177–201

[49] Williams R O and Paxton H W 1958 *Trans. Am. Inst. Min. Metall. Pet. Eng.* **212** 422–23

[50] Messoloras S, Pike B C, Stewart R J and Windsor C G 1984 Precipitation in iron–chromium–aluminium alloys *Metal Sci.* **18** 311–21

[51] de Carlan Y, Alamo A, Mathon M H, Geoffroy G and Castaing A 2000 "Effect of thermal aging on the

microstructure and mechanical properties of 7–11 CrW steels *J. Nucl. Mater.* **283–7** 672–6

[52] Dubuisson P, Gilbon D and Séran J L 1993 Microstructural evolution of ferritic-martensitic steels irradiated in the fast breeder reactor Phénix *J. Nucl. Mater.* **205** 178–89

[53] Alamo A, Lambard V, Averty X and Mathon M H 2004 Assessment of ODS-14%Cr ferritic alloy for high temperature applications *J. Nucl. Mater.* **329–33** 333–7

[54] Reese E R, Almirall N, Yamamoto T, Tumey S, Robert Odette G and Marquis E A 2018 Dose rate dependence of Cr precipitation in an ion-irradiated Fe–18Cr alloy *Scr. Mater.* **146** 213–7

[55] Pareige C, Kuksenko V and Pareige P 2015 Behaviour of P, Si, Ni impurities and Cr in self ion irradiated Fe–Cr alloys—comparison to neutron irradiation *J. Nucl. Mater.* **456** 471–6

[56] Kahlweit M 1975 Ostwald ripening of precipitates *Adv. Coll. Interface Sci.* **5** 1–35

[57] Lifshitz I M and Slyozov V V 1961 The kinetics of precipitation from supersaturated solid solutions *J. Phys. Chem. Solids* **19** 35–50